공학석사 학위논문

Enhancement of Light Extraction Efficiency of Organic Light Emitting Diodes using Spin-on Glass based Randomly Dispersed Nano-pillar Arrays

유기 발광 다이오드의 광추출 효율 향상을 위한 스핀 온 글라스로 만든 비주기적 나노 구조

2013년 2월

서울대학교 대학원
재료공학부
한 경 훈

Enhancement of Light Extraction Efficiency of Organic Light Emitting Diodes using Spin-on Glass based Randomly Dispersed Nano-pillar Arrays

유기 발광 다이오드의 광추출 효율 향상을 위한 스핀 온 글라스로 만든 비주기적 나노 구조

지도 교수 김 장 주

이 논문을 공학석사 학위논문으로 제출함

2013 년 2 월

서울대학교 대학원

재료공학부

한경훈

한경훈의 석사 학위논문을 인준함

2013 년 2 월

위 원 장	윤재륜	(인)
부위원장	김장주	(인)
위 원	서용석	(인)

Abstract

Enhancement of Light Extraction Efficiency of Organic Light Emitting Diodes using Spin-on Glass based Randomly Dispersed Nano-pillar Arrays

Kyoung-Hoon Han

Department of Material Science & Engineering

The Graduate School

Seoul National University

Randomly dispersed nano-pillar array (RaDNA) was embedded between the transparent electrode and the glass substrate to extract lights confined inside organic light emitting diodes (OLED). The room-temperature nano-imprining lithography (RT-NIL) was employed for the fabrication of RaDNA. Spin-on glass was utilized as a material of the nano-pillar array for stable devices. The pillar arrays were planarized before fabrication of OLEDs using a high refractive index material (trialkoxysilane-capped PMMA-titania hybrid optical material) to reduce the leakage current. The

RaDNA OLED showed 7% enhancement in normal direction and 19% enhancement of light extraction efficiency in an integrating sphere. The emission pattern of RaDNA device showed no variation of emission spectrum with azimuthal angle and viewing angle.

Keywords: Organic light emitting diode, Randomly dispersed nano-pillar array, Spin-on glass, Room temperature nano-imprinting lithography, trialkoxysilane-capped PMMA-titania hybrid optical material.

Student Number: 2011-22874

Contents

List of Tables

List of Figures

Chapter.1

Introduction

1.1 Organic light emitting diodes: principle and limitation of efficiency

Organic light emitting diodes (OLEDs) have been an attractive research area for solid-state lighting because of low power consumption, good color and potentially low price etc. Figure 1.1a shows the conventional structure of OLEDs which is composed of glass substrate, transparent anode, hole transporting layer (HTL), light emitting layer (EML), electron transporting layer (ETL) and reflective cathode.

The schematic energy-level diagram of an OLED is shown in Figure 1.1b. When a voltage is applied in the OLED, electrons are injected into the lowest unoccupied molecular orbital (LUMO) level of the ETL from the anode and holes are injected into the highest occupied molecular orbital (HOMO) level of the HTL from the cathode. In the EML, holes and electrons approach each other and recombine to form excitons. Then, light is generated by the radiative decay of excitons.

The efficiency of an OLED can be expressed as follow: [1, 2]

$$\eta_{ext} = (\gamma \times \eta_{exc} \times q) \times \eta_{out} = \eta_{int} \times \eta_{out} \qquad (1.1)$$

Where γ is the electron–hole charge balance factor. $\eta_{S/T}$ is the singlet-triplet

factor ($\eta_{S/T}$ ~0.25, and ~1 for fluorescence, and phosphorescence EML materials, respectively) and q is the quantum yield, η_{out} is the outcoupling efficiency of the emitted light, and η_{int} is the internal quantum efficiency,. Despite η_{int} can reach around 1 through a proper design of device structure and selection of an efficient phosphorescent material, η_{out}, the ratio of the number of photons extracted through the front face of device to the number of photons generated in an OLED is at most 20~30%. Large portion of the emitted light is confined in the OLED in glass substrate (n=1.4 ~ 1.5), transparent electrode (n=1.8 ~ 2.0) and organic layer (n=1.7 ~ 1.8), or dissipated as surface plasmon polaritons as shown in Figure 1.2. From ray optics[2], 50% of the emitted light is trapped in the organic and ITO layer (waveguide mode) and 30% is trapped in glass substrate (substrate mode). Only 20% of the generated light in the OLED is extracted to air (air mode).

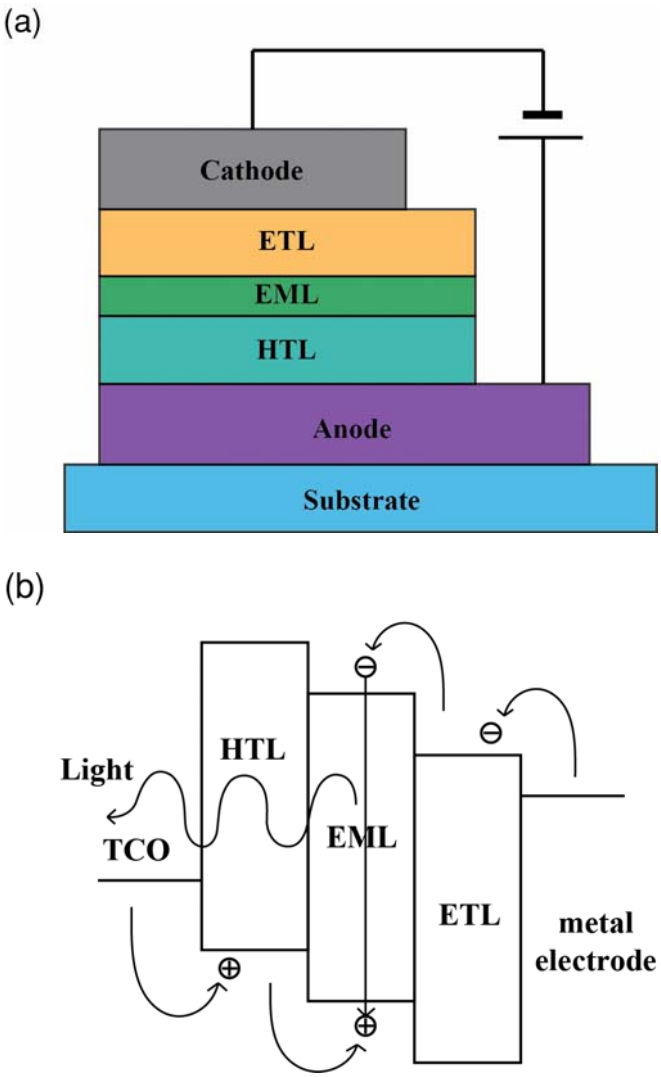

Figure 1.1 (a) The basic structure of OLEDs. (b) The schematic diagram of the energy level of OLEDs.

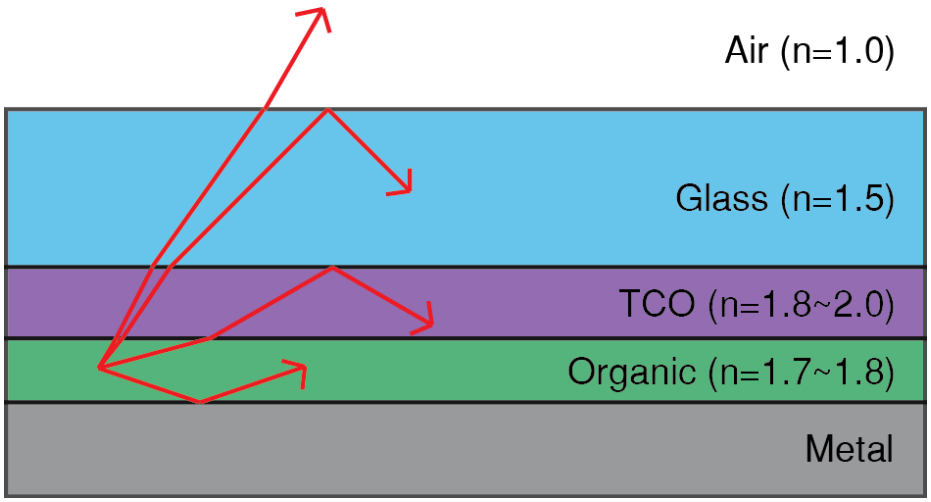

Figure 1.2 Schematic diagram of coupling modes of emitted light in an OLED.

1.2 OLEDs with randomly dispersed nano-pillar array (RaDNA)

Many methods have been reported to increase η_{out}. Those methods can be classified into two types by targetting modes. The first category is the modification of the substrate, such as textured surface [2], meshed surface [3] and micro lens array [4] to extracting light trapped in the glass substrate. The outcoupling efficiency of 50% was achieved using the methods [2-4]. These processes are simple. However, they have limitations in the enhancement of the outcouplung efficiency because they can extract light confined in the substrate. Moreover, they give high haze resulting in pixel blur [4]. The other category is to extract the wave-guided mode, which include 2-D photonic crystal (PC) [5-8], low index grid [9], aperiodic dielectric mirror [10], ITO nano-structure [11], silica micro sphere as scattering medium [12] etc. Higher enhancement ratio can be achieved using the later methods in principle at the expense of complicated process [6, 7, 11, 12], distorted spectrum [5, 13], intensity variation along viewing angles [6-9], degradation of electric property [10], and limited aperture ratio [10].

Among the methods, the PC structure has a potential strength because of a simple process and a high enhancement [9]. The PC structure is composed of substrate, nano-pillar array, planarization layer and, an OLED is integrated on the top of the PC structure (PC-OLED) as shown in figure 1.3. The diameter and height of pillar and the distance between the pillars were sub-wavelength [13]. To achieve a high enhancement, pillars were distributed as hexagonal array. The enhancement of 58% was achieved [9].

However, the PC structure with periodic pillar array has drawbacks of non-uniform enhancement of outcoupling along the azimuthal angle and viwing angle due to the diffraction. To achieve an uniform emission pattern, Cho [14] and Park [15] implemented the Randomly Dispersed Nano-pillar Array (RaDNA) whose SEM images of the patterns are shown in Figure 1.4. Nano-pillars with different diameters were dispersed randomly in 10 * 10 μm^2. The random patterns were repeated in tetragonal periodicity. The pattern types were named as A to D by the degree of randomness. Enhancement of 84% was achieved [16].

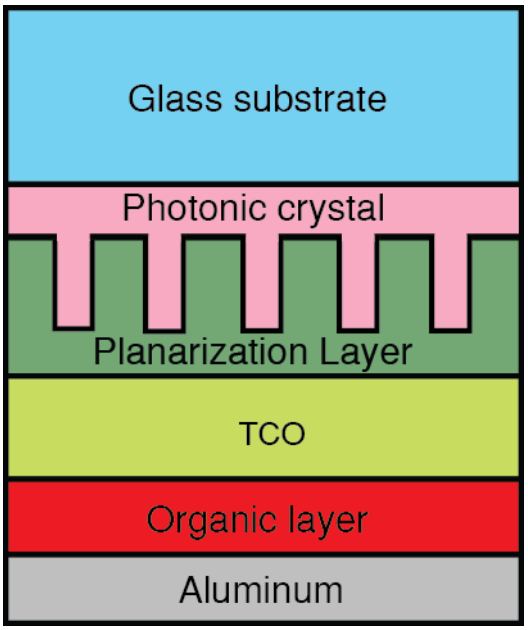

Figure 1.3 Schematic diagram of an OLED with a photonic crystal structure.

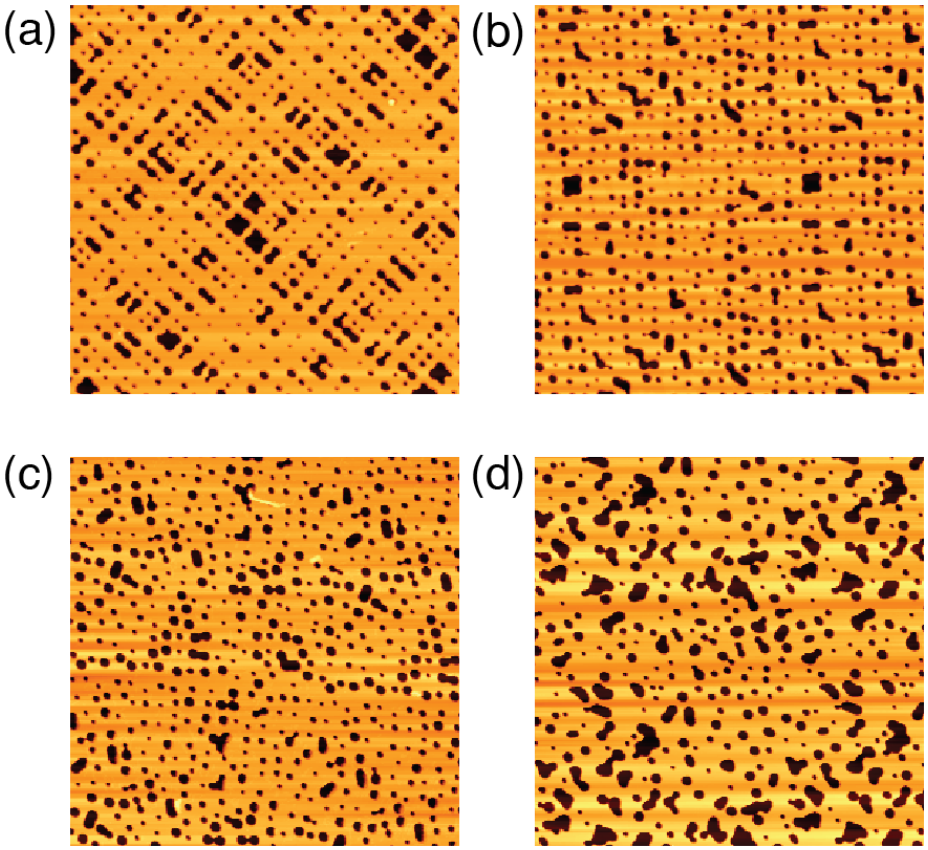

Figure 1.4 AFM images of RaDNA molds. (a) Pattern A, (b) pattern B, (c) pattern C, (d) pattern D.

1.3 Spin-on glass

The material of pillar must be considered carefully in the PC OLEDs. Materials which have been used for the fabrication of PC structures are summarized in Table 1. Each material has advantages and disadvantages. For example, SiO_2 and SiN_x have large difference in refractive indices between them to give large reflection at the interface but they were fabricated by expensive PECVD and reactive ion etching lithography [6, 7]. The UV curable resin has a simple process and a high formability [8, 9, 16]. However the material requires an out-gassing problem which is detrimental to the life time of OLEDs and is not very stable under high temperature process which is needed to device.

In this thesis, spin-on glass (SOG) is chosen as the pillar material. The SOG has been originally utilized as a planarization layer in the multi-layered semiconductor device and is composed of SiO_2 sol-gel (usually alkoxysilane) and organic solvents (usually alcohol). After spin coating, the SOG gel layer is formed on the substrate. During baking, the SOG gel layer is transformed to the rigid SiO_2 layer. The reaction equation of hydrolyzation and polymerization of alkoxysilane are shown below [16].

$$\equiv Si - O - C_2H_5 + H_2O \Rightarrow \equiv Si - OH + C_2H_5OH$$

$$\equiv Si - O - C_2H_5 + \equiv Si - OH \Rightarrow \equiv Si - O - Si\equiv + C_2H_5OH$$

Finally, annealing process is followed to eliminate the organic residue.

Dense and stable SiO_2 film is formed. The advantages of SOG pillar array are (i) same refractive index with glass, (ii) stability at high temperature and (iii) high durability.

Recently, the nano-structure of SOG was fabricated by nano-imprinting lithography (NIL) at room temperature, indicating that the process of SOG can be simple with high formability.

Table 1.1 Lists of materials used for pillar and planarization layer from literatures.

pillar material	**Planarization material**	**Enhancement of efficiency**	**Pattern type**	**Ref. No.**
SiO_2	SiN_x	85%	Tetragonal PC, 200 nm	5
SiN_x	Spin-on glass	85%	Tetragonal PC, 300 nm	6
UV-curable resin	SiN_x	50%	Hexagonal PC, 265 nm	7
UV-curable resin	TiO_2 (sol-gel)	58.2%	Hexagonal PC, 300 nm	8
UV-curable resin	polymer-TiO_2 hybrid polymer	82%	RaDNA, 300 nm	15

Chapter.2

Fabrication of SOG RaDNA

2.1 Introduction

The SOG nano-structure was fabricated with NIL. The principle of NIL is a deformation of resin by mechanical force [17]. In comparison with the nano-fabricating methods, NIL has strong advantages which are simple and chip process, high throughput, and high precision etc. [18] Matsui et al. achieved room temperature SOG NIL at 2.5 Mpa [17]. However, the pressure during processing for imprinting is too high, because SOG hardens fast due to the reaction with air. To reduce the pressure, the soft-NIL with the elastic mold like PDMS is reported [18]. Using the PDMS mold has some merits: (i) the absorption of organic solvent that can help in anti-sticking, (ii) the high gas permeability which makes possible to have little deformation during NIL in evaporation of solvent, (iii) the large conformal contact area which needs low pressure, (iv) the low surface energy which makes de-molding process simple [19]. Despite of using the PDMS mold, the pressure of imprinting is still high because of the SOG hardening. To avoid this problem, the reverse NIL (nano-transferring) was utilized in this experiment. The reverse NIL is that resin is deposited on the mold and then nano-structured layer was transferred to the substrate [20].

2.2 Fabrication of RaDNA substrate

The PDMS mold was fabricated from the UV curable resin RaDNA substrate, namely the fabrication of the UV curable resin RaDNA substrate was preceded.

First, the Si master molds were fabricated by E-beam lithography. The self-assembling monolayer (SAM), trichloro-1H, 1H, 2H, 2H-fluorooctyl silane (Aldrich) was formed on surface of mold to easily detach the UV-curable resin on a glass substrate. The SAM was vapor-deposited at 60 mmHg for 30 min [21], thereby creating a low surface energy of mold. Before the NIL process, hexamethyldisilazane (ZAP-1020, Chemoptics) was deposited by spin coating on the glass substrate to enhance the adhesion of the resin. The UV curable resin is an acrylate polymer with the photo-initiator. After dropping of 5 μl of the UV curable resin on Si mold, the mold was covered by the glass. The stack of glass/resin/mold was exposed to UV radiation with 14 mw/cm^2 for 310s, and the mold was detached from patterned substrate.

Figure 2.1 is a schematic diagram of process including fabrication of the PDMS mold, the NIL of SOG and the annealing substrate. To fabricate the PDMS mold, Sylgard 184 silicone, a two-part PDMS elastomer was purchased from Dow corning. 10:1 (by volume) mixture of the PDMS base/curing agent was degassed with the RaDNA substrate under vacuum for 2 hours and cured at 80°C for 4 hours. After curing, the PDMS replica mold was detached from the RaDNA substrate.

The concentration of SOG solution (SOG 15A, Filmtronics) was doubled by vaporization to prevent rapid evaporation of solvent during spin-coating. If

the concentration of solvent is high, a bubble strain is formed on the mold after spin coating. The SOG was deposited by spin coating on the PDMS mold at 5000 rpm for 10 sec, followed by covering on the glass substrate. The Stack of the mold/SOG/glass was pressed to completely fill a gap between the mold and the substrate at 5 bar and room temperature and vacuum for 10 min. After demolding, the SOG RaDNA substrate was annealed at 400°C for 1 hour at vacuum to eliminate the debris.

Whole processing method looks like long and complicated. Once the UV curable resin RaDNA is fabricated, it can be used many times. So, forming the PDMS mold is actual first experimental step.

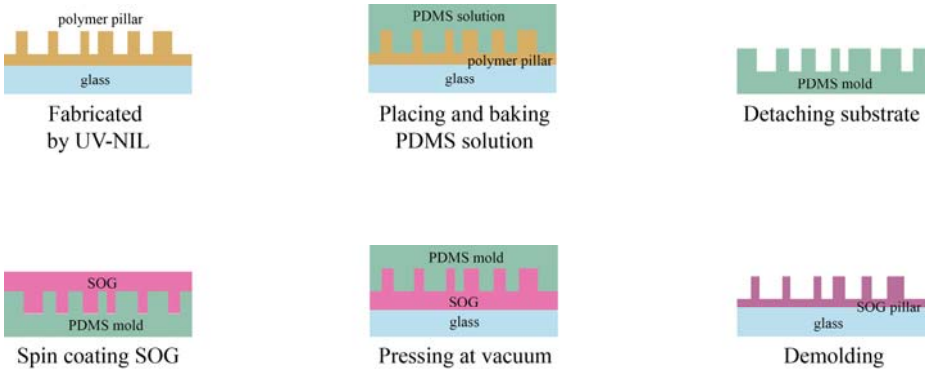

Figure 2.1 Schematic diagram of the fabrication of RaDNA using the nano-imprint lithography.

2.3 Planarization of RaDNA substrate

Before deposition of OLED, RaDNA substrate must be planarized. Pillar array can be leakage path in OLED because height of pillar is higher than organic layers of OLED. In this thesis, the trialkoxysilane-capped PMMA-titania hybrid optical material which was synthesized by Lee et al. was used for planarization [22].

To planarize the RaDNA substrate, the trialkoxysilane-capped PMMA-titania hybrid optical material was utilized [22]. The material formula is shown in Figure 2.2. Through the acid-catalyst-free polymerization, the hybrid material could have high titania contents. In this thesis, titania contents of 75 wt% (T75) was utilized. The refractive index of T75 is 1.71~1.82. The T75 was deposited by spin coating onto the RaDNA substrate at 1000 rpm, 30 sec. and baked at 230℃ for 10 min.

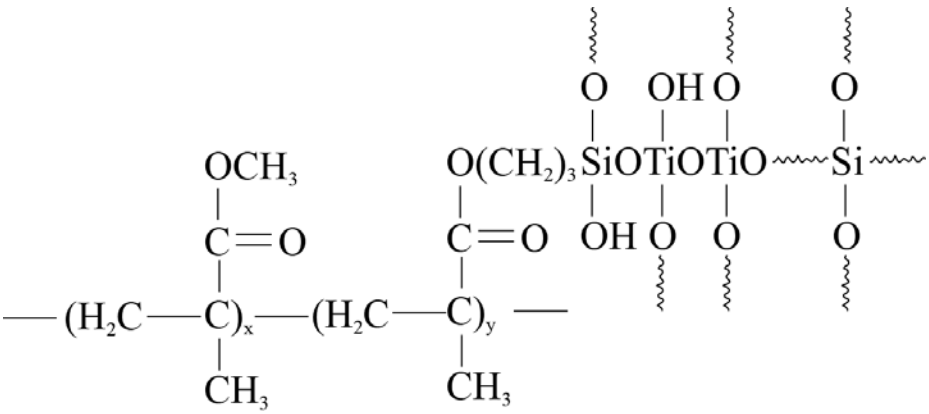

Figure 2.2 Structural formula of trialkoxysilane-capped PMMA-titania hybrid.

2.4 Characterization of RaDNA substrate

To figure out the characterization of the SOG substrate, various measurements were performed. The images of RaDNA substrate were measured by optical microscope, atomic force microscope (AFM), scanning electron microscope (SEM). In addition to the images, the transmittance and the haze of the substrate were measured.

Figure 2.3 shows the AFM image of the UV-curable resin RaDNA substrate whose pattern is almost reverse pattern of Si master mold. So the UV-curable resin RaDNA substrate has equal heights of nano-pillar.

The AFM image SOG RaDNA after NIL is shown in Figure 2.4. The heights and the diameters of the SOG pillar were lower than the UV curable pillar's. During NIL, the SOG pillar heights were decreased due to the evaporation of solvents. Figure 2.5 shows AFM image of the SOG RaDNA substrate after annealing. Through annealing, the gel pillar was converted to the poly-crystalline SiO_2 pillar with densification and grain growth. Despite of the shrinkage of the pillar diameter, the average pillar height was remained as 225 nm during curing process. The shrinkage was taken up in the dimension mainly perpendicular to the surface [17]. The AFM image of the planarized substrate is in Figure 2.6. The mean pillar radius and roughness of substrates was obtained as in table 2. The R_{pv} of RaDNA substrates before and after planarization were 299 nm and 243 nm.

Figure 2.7 and Figure 2.8 show the optical microscope images of RaDNA substrates before and after planarization. Periodic 10 * 10 μm^2 random patterns can be seen in large area. The T75 didn't make substrate totally flat,

so nano-pattern also was shown in the planarized substrate. Instead of the rough surface, any crack was shown in the planarized substrate.

The SEM images of the substrate before and after planarization are shown in Figure 2.9. Different material could be discerned by different electron back scattering. Fig 2.9 (a), around 300 nm of SOG thin layer was deposited on the glass substrate except pillar array. Around 140nm of the T75 thin film was coated on pillar array as shown in Fig 2.9 (b). The roughness of the planarized substrate was due to lower thickness of the T75 film than the height of the SOG pillar.

To be applied in a display, the transmittance haze that is related with a pixel blurring is also key-factor to be considered. Figure 2.10 shows measurement system of transmittance haze. The transmittance haze is percent ratio of the diffused transmittance to the total transmittance in integrating sphere. The result of haze measurement with white light is shown in table 2.2. Higher pillar height has more capability of light-scattering so, had bigger haze. The haze of SOG substrate was lower than UV curable resin's due to lower pillar height. The hazes of RaDNA substrates before and after planarization were 13.12 and 3.49. Figure 2.11 (a) ~ (d) are photographs of text printed beneath different substrates (glass substrate, planarized SOG RaDNA substrate, UV curable resin substrate, microlens array on the glass substrate). Thickness of glass substrate is 0.64 mm. Texts beneath microlens array on substrate were blurred. While texts beneath planarized SOG RaDNA substrate were clear and it means SOG RaDNA substrate is more proper at a display.

The transmittance of substrate is shown in Figure 2.12. Because of light-

scattering, transmittance of RaDNA substrate was lower than transmittance of bare glass. Planarized RaDNA substrate had higher transmittance than RaDNA substrate at 480 ~ 520 nm, green light.

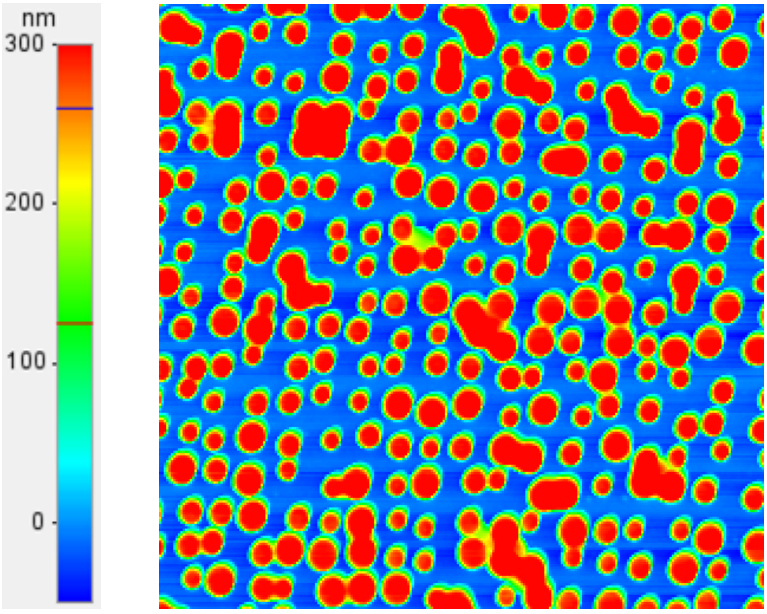

Figure 2.3 AFM image of RaDNA substrate fabricated using a UV curable resin.

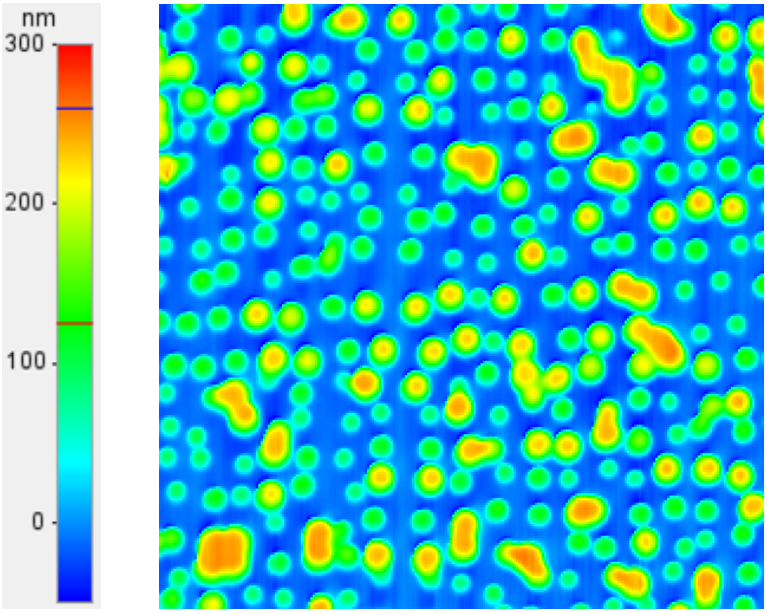

Figure 2.4 AFM image of SOG RaDNA substrate fabricated using SOG.

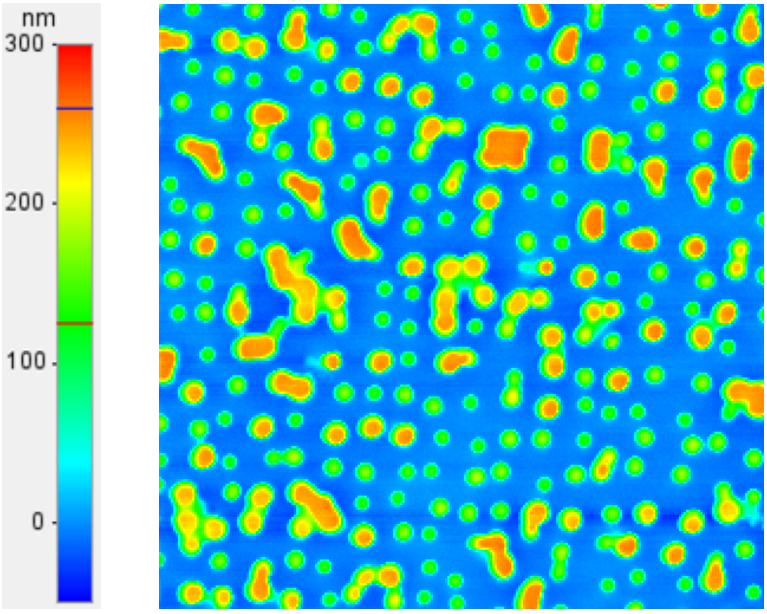

Figure 2.5 AFM image of SOG RaDNA substrate after curing at 400°C and vacuum for 1 hour.

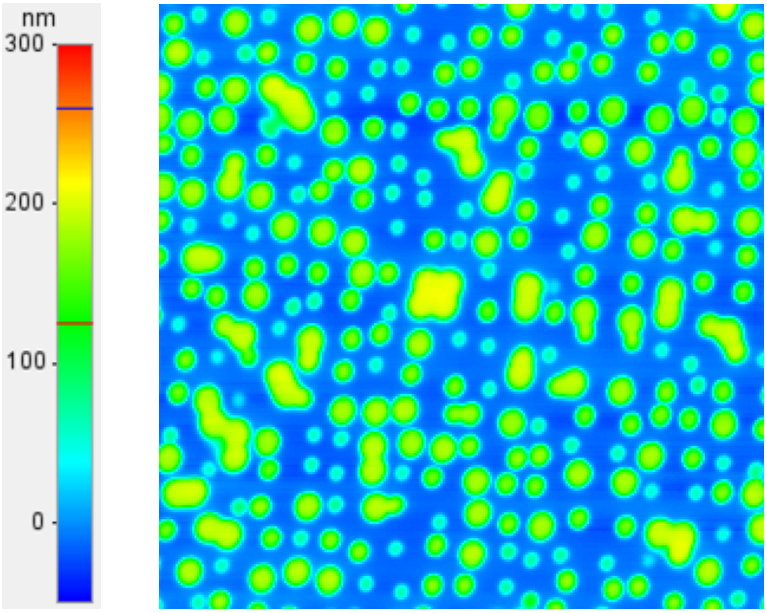

Figure 2.6 AFM image of SOG RaDNA substrate planarized by T75.

Table 2.2 Summary of area, volume, height, peak to valley of pillars.

Substrate	**Average radius (nm)**	**R_{pv} (nm)**	**R_q (nm)**	**R_a (nm)**
RaDNA (UV-curable resin)	227	407	140	131
RaDNA (SOG)	209	324	77.7	64.3
RaDNA (SOG, cured.)	185	299	82.2	67.6
RaDNA (SOG, planarized.)	197	243	68.74	57.7

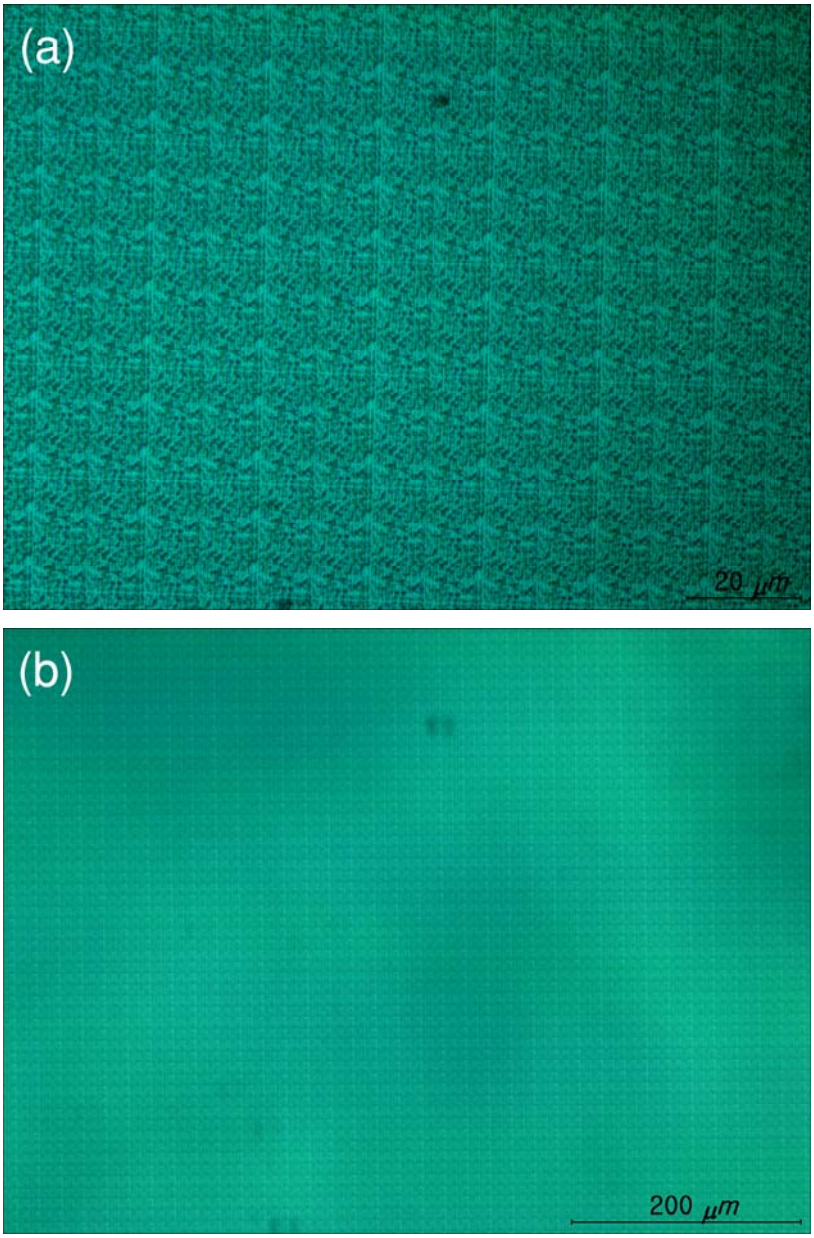

Figure 2.7 Optical microscope image of RaDNA substrate at magnification of (a) x 500 and (b) x 100.

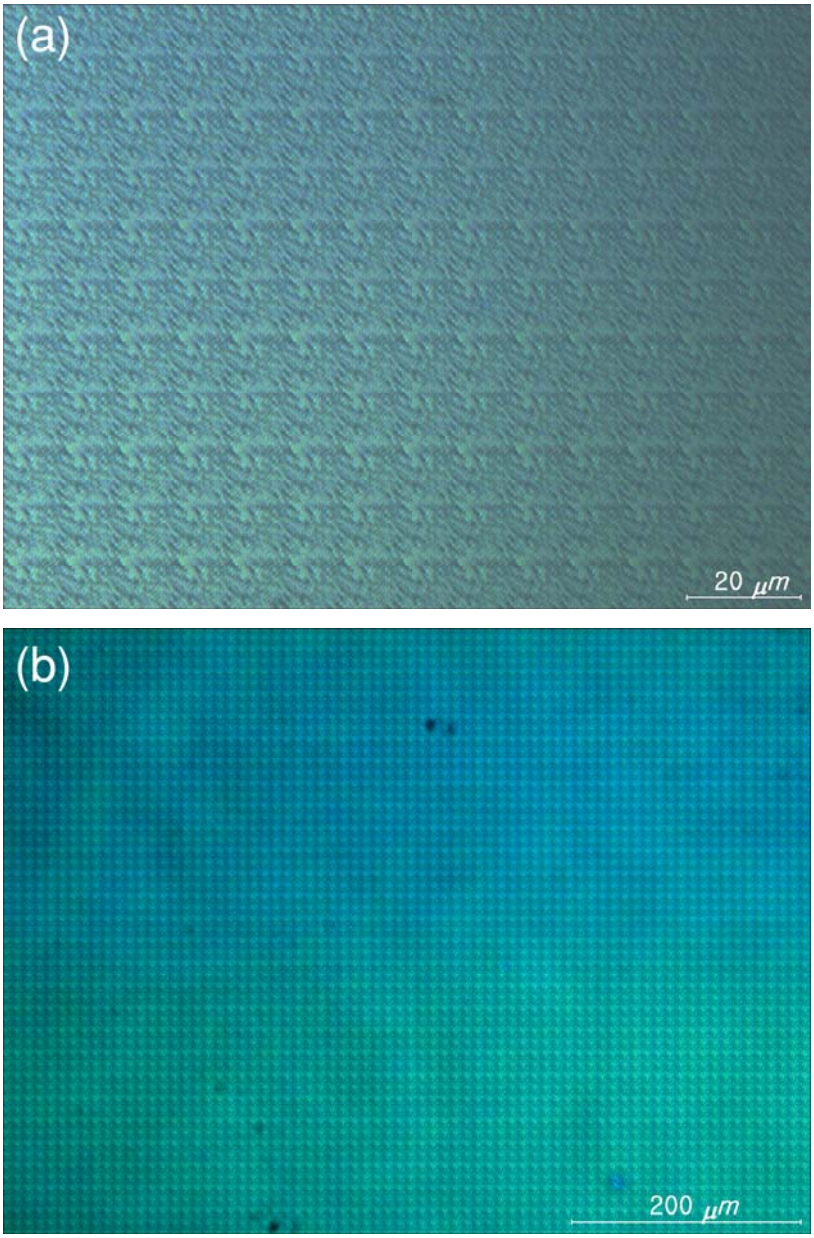

Figure 2.8 Optical microscope image of planarized RaDNA substrate at magnification of (a) x 500 and (b) x 100.

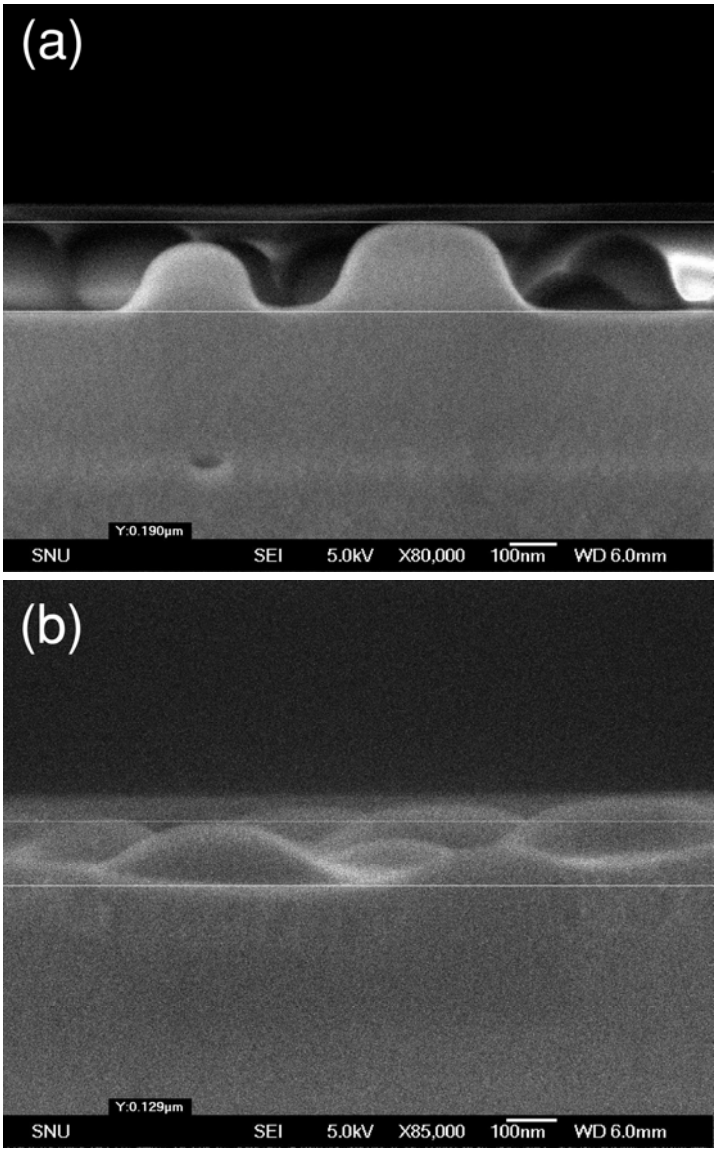

Figure 2.9 SEM images of RaDNA substrate before and after planarization.

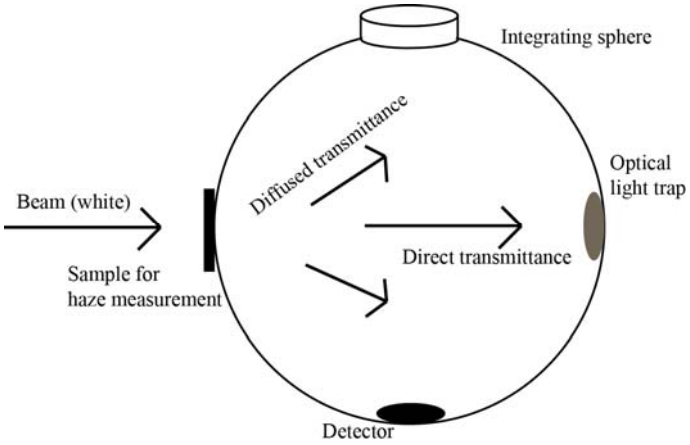

Figure 2.10 Schematic measurement system of transmittance haze in integrating sphere.

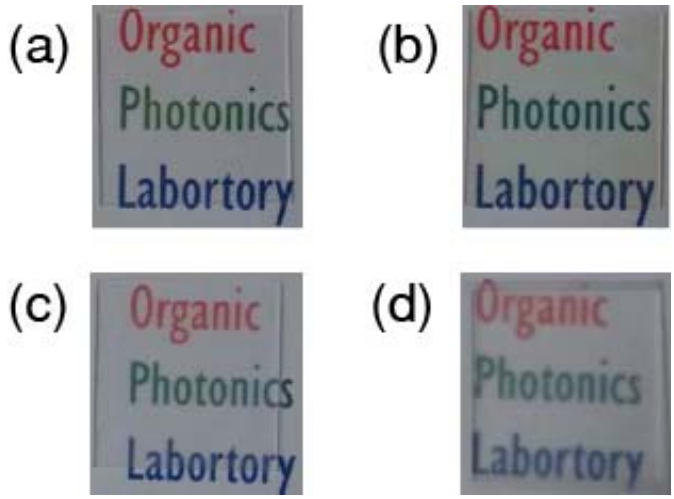

Figure 2.11 Photographs of images througn (a) glass substrate, (b) planarized SOG RaDNA substrate, (c) UV curable resin substrate and (d) microlens array on the glass substrate.

Table 2.3 Haze and transmittance of RaDNA substrates with different material and height of pillar before and after planarization.

Substrate	Planarization	Height of pillar	Transmittance	Haze
Glass	X	0	92.08	0.14
UV curable resin RaDNA substrate	X	70	91.84	2.05
UV curable resin RaDNA substrate	X	150	90.68	8.09
UV curable resin RaDNA substrate	X	300	87.85	35.09
SOG RaDNA substrate	X	300	91.72	13.12
UV curable resin RaDNA substrate	O	70	87.5	0.48
UV curable resin RaDNA substrate	O	150	86.33	0.8
UV curable resin RaDNA substrate	O	300	84.27	2.52
SOG RaDNA substrate	O	300	87.09	3.49

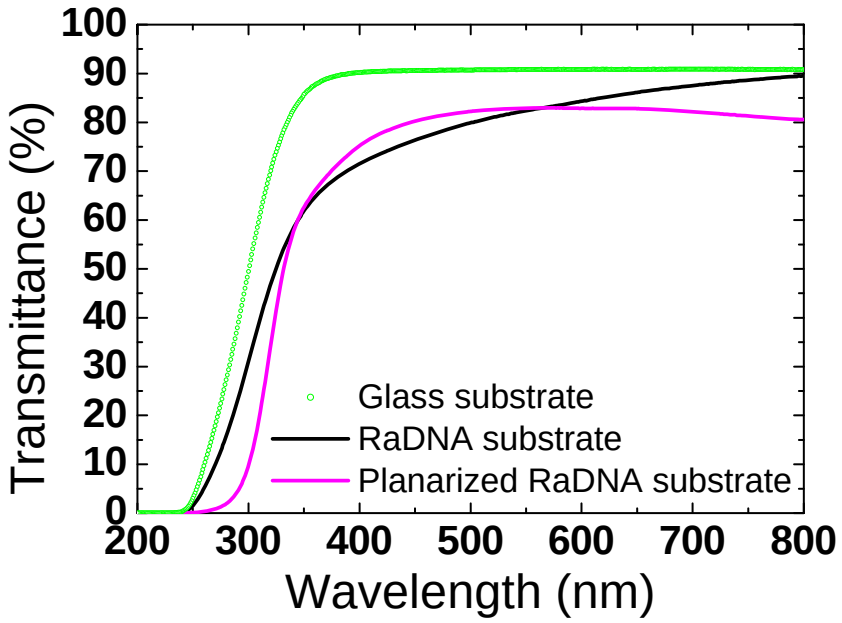

Figure 2.12 Transmittance of glass and RaDNA substrate before and after planarization.

Chapter.3

Fabrication of RaDNA OLED

3.1 Device design of green phosphorescent OLED

The OLED structure is highly efficient green phosphorescent device that was devised by Lu et al. [23]. In this device, using CBP as both HTL and EML, energy barrier between HTL/EML was eliminated. Nearly same Energy level of the ETL (TPBi) with the EML (CBP) made the device have good roll-off.

In contrast to the original device, transparent electrode material is used as indium zinc oxide (IZO). Because transparent electrode has different refractive index and thickness, OLED device was re-designed to have a high efficiency. The optimization of device was performed with a classical electromagnetic theory developed by Chance, Prock and Silbey (CPS) [24, 25]. In simulation, device was modeled as a simple one dimensional (1D) weak micro-cavity which consists of glass, IZO, multi-layered organic and metal. The emission was assumed as isotropic sheet dipole radiation which is located in the center of the EML. Thickness of the HTL was systemically changed to watch power coupling ratios without changing thickness of other layers. The Schematic diagram of the device structure for optical modeling is shown in Figure 3.1.

Figure 3.2 shows the simulation result from different HTL thickness. When the HTL thickness is 70 nm, 25% out-coupling efficiency was achieved. The fraction of internal absorption, surface plasma polariton (SPP), organic mode,

wave guide mode was 0.11, 0.11, 0.37 and, 0.16. The SPP is absorption due to dipole decay near metal. Each material has imaginary refractive indices, 11% light is absorbed. Due to the high refractive indices of organic and IZO, 37% of generated light in device was captured still.

Optimized device structure was IZO (70 nm) / MoO_3 (1 nm) / CBP (75 nm) / CBP : 8wt.% $Ir(ppy)_2(acac)$ (15 nm) / TPBi (60 nm) / LiF (1 nm) / Al (100 nm)

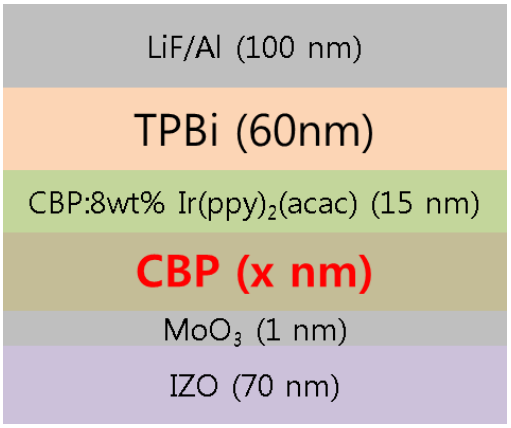

Figure 3.1 Schematic diagram of the device structure for optical modeling.

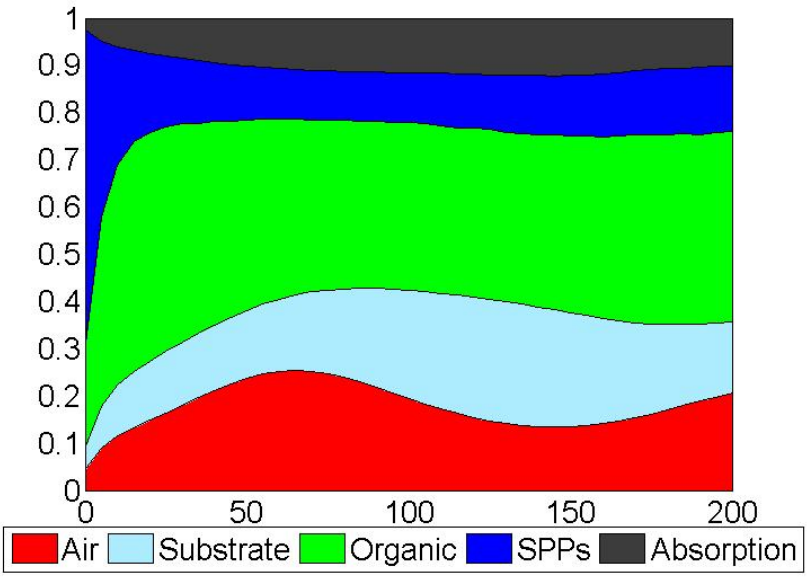

Figure 3.2 Power coupling ratio of the dissipated power from emissive dipoles coupled to various optical modes.

3.2 Fabrication of green phosphorescent OLED

The OLED was fabricated on the planarized RaDNA substrate as optimized device. The IZO was deposited by a facing target sputtering system at working pressure $2.5*10^{-3}$ Torr. The sheet resistance of the IZO was measured by 4-point probe and has 103 Ω/□. Before the organic deposition, UV-O_3 treatment was done for 10 min on the IZO electrode to reduce the energy level of IZO. Organic materials were deposited by the thermal evaporation without breaking the vacuum at a pressure of $< 5*10^{-7}$ Torr. The thickness of each layer was measured by a quartz crystal sensor. For comparison with conventional ITO device, ITO substrate also fabricated along with IZO device. A Keithley 2400 semiconductor parameter analyzer and a Photo Research PR-650 spectrophotometer were used to measure the luminescent and electric characteristics, respectively. The integrating sphere with a photomultiplier was utilized for measurement of total extraction enhancement.

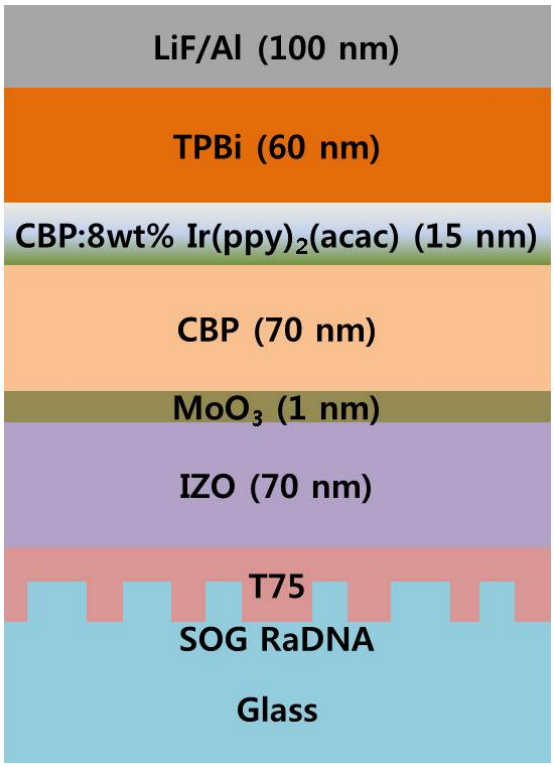

Figure 3.3 The structure of RaDNA OLED.

3.3 Result and Discussion

The current density-voltage-luminance (J-V-L) diagram is shown in Figure 3.4. All devices have 3 V of turn-on voltage. That means OLED had been fabricated equally. In high voltage, current density of IZO device was lower than ITO device's due to high sheet resistance of IZO. The reason that the RaDNA OLED has high injection properties was roughness of the RaDNA substrate. The electrode on pillar was applied high electric field. That results in large current injection.

Figure 3.5 shows luminance efficiency and power efficiency of reference and RaDNA device. The luminance efficiency at 2.5 mA/cm^2 are 98.41 (reference) and 105.47 (RaDNA) Cd/A. The power efficiency at 2.5 mA/cm^2 are 50.66 (reference) and 57.89 (RaDNA) lm/watt. The enhancement ratio of luminance efficiency and power efficiency were 1.07 (luminance efficiency) and 1.14 (power efficiency).

Figure 3.6 shows the result of integrating sphere measurement at 2.5 mA/cm^2. The spectrum of both reference and RaDNA OLED were almost same. Overall enhancement ratio was larger in integrating sphere. It was inferred that lights of high angle at normal direction were extracted more. The increase of glass mode of light was inferred from larger enhancement at high angle.

The enhancement ratio of each wavelength is shown in Figure 3.7. The electroluminescence (EL) intensity at edge sides was so low that the enhancement at both sides can't be accepted as it shows. In contrast to the PC OLED, the enhancement ratio was equal at each wavelength. It means the

RaDNA OLED shows any color-shift.

Overall enhancement ratio has lower value than hexagonal PC OLED's. PC OLED was optimized to enhance light of specific wavelength. In contrast to variation with viewing angle of PC OLED, RaDNA OLED has equal emission pattern.

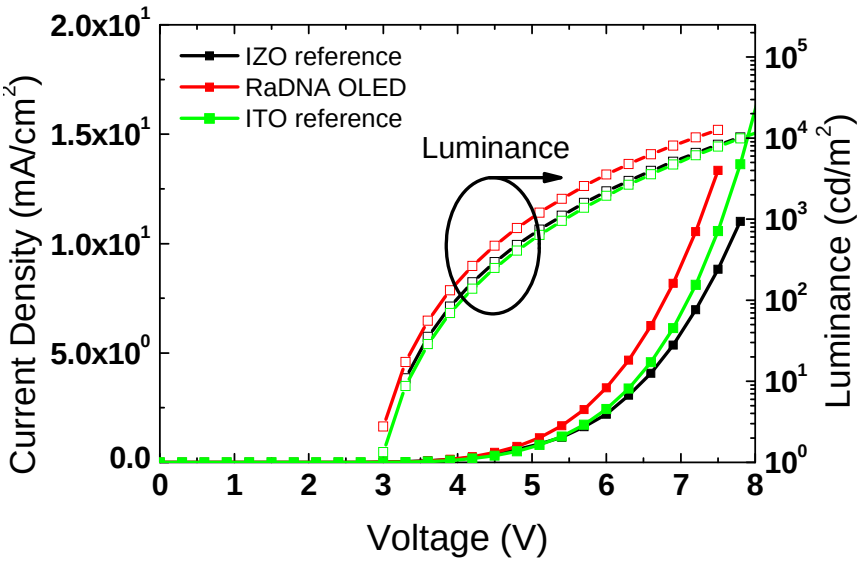

Figure 3.4 Current density-voltage-luminance characteristics.

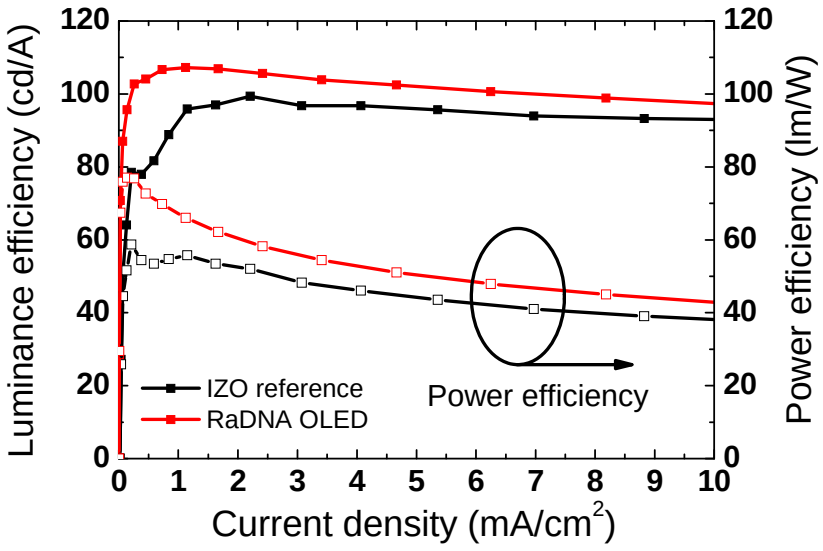

Figure 3.5 Luminance and power efficiency curve.

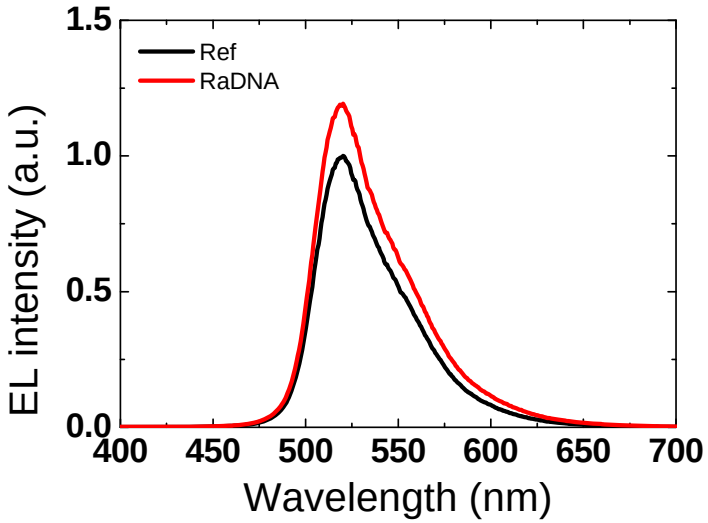

Figure 3.6 The EL intensity at integrating sphere.

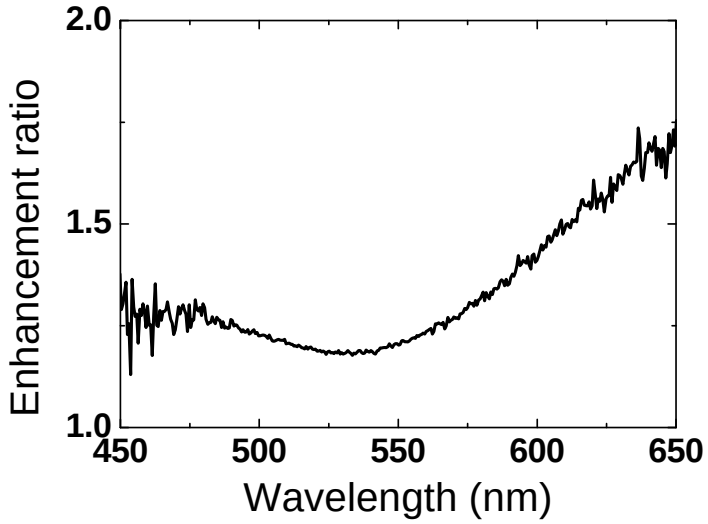

Figure 3.7 Enhancement ratios at wavelength

Chapter.4

Conclusion

The RaDNA substrate was fabricated with the spin-on glass. The fabrication method was simple with the RT-NIL. The trialkoxysilane-capped PMMA-titania hybrid optical material was used as planarization layer, decreasing peak to valley 299 nm to 243 nm and had no crack. The planarized substrate showed haze less than 10. The optimized OLED was designed with CPS simulation which is based on the classical electromagnetic theory. The RaDNA OLED has 7% efficiency enhancement at normal direction and 19% enhancement in integrating sphere. The emission pattern didn’t show any variation with azimuthal angle.

References

[1] S.R. Forrest, D.D.C. Bradley, M.E. Thomson, Adv. Mater. **15,** 1043 (2003).

[2] N.K. Patel, S. Cinà, J.H. Burroughes, IEEE J. on Selected Topics in Quantum Electronics, **8**, 346 (2002).

[3] Y.-H. Cheng, J.-L. Wu, C.-H. Cheng, K.-C. Syao and M.-C. M. Lee, Appl. Phys. Lett. **90**, 091102 (2007).

[4] S. Möller and S. R. Forrest, J. Appl. Phys. **91,** 3324 (2002).

[5] Y.-R. Do, Y.-C. Kim, Y.-W. Song, C.-O. Cho, H. Jeon, Y.-J. Lee, S.-H. Kim and Y.-H. Lee, Adv. Mater. **15**, 1214 (2003).

[6] Y.-C. Kim, S.-H. Cho, Y.-W. Song, Y.-J. Lee, Y.-H. Lee, Y. -R. Do, Appl. Phys. Lett. **89**, 173502 (2006).

[7] S.-H. Jeon, J.-W. Kang, H.-D. Park, Jang-Joo Kim, J.-R. Youn, J.-Y Shim, J.-H Jeong, D.-G. Choi, K.-D. Kim, A. O. Altun, S.-H. Kim, and Y.-H. Lee, Appl. Phys. Lett. **92**, 223307 (2008).

[8] H.-H. Cho, B.-I. Park, H.-J. Kim, J.-Y. Shim, S.-H. Jeon, J.-H. Jeong, J.-J. Kim, Curr. Appl. Phys. **10**, e139 (2010).

[9] Y. Sun and S. R. Forrest, Nat. Photonics, **2**, 483 (2008).

[10] S.A. Choulis, M.K. Mathai, and V.E. Choong, Appl. Phys. Lett. **88**, 213503 (2006).

[11] A. Kumar, R. Srivastava, M. N. Kamalasanan, and D. S. Mehta, Opt. Lett. **37**, 575 (2012).

[12] T. Yamasaki, K. Sumioka, T. Tsutsui, Appl. Phys. Lett. **76,** 1243 (2000).

[13] Y.-J. Lee, S.-H. Kim, G.-H. Kim, Y.-H. Lee, S.-H. Cho, Y.-W. Song, Y.-C. Kim, Y.-R. Do, Opt. Express **13**, 5864 (2005).

[14] H.-H. Cho, mater thesis, SNU (2009).
[15] B.-I. Park, mater thesis, SNU (2011).
[16] N. N. Toan, thesis, University of Twente (1999).
[17] L. J. Guo, Adv. Mater. **19**, 495, (2007).
[18] Y. Kang, M. Okada, C. Minari, K. Kanda, Y. Haruyama and S. Matsui, Jpn J. Appl. Phys. 49, 06GL13 (2010).
[19] Y. Xia and G. M. Whitesides, Angew. Chem. Int. Ed. **37**, 550 (1998).
[20] K.-Y. Yang, S.-C. Oh, H. Park, and H. Lee, J. Vac. Sci. Technol. B **29**, 051602 (2011).
[21] H.-C. Scheer, W. Häfner, A. Fidler, S. Möllenbeck, and N. Bogdanski, J. Vac. Sci. Technol. B, **26(6)**, 2380 (2008).
[22] L.-H. Lee and W.-C. Chen, Chem. Mater. **13**, 1137 (2001).
[23] Z. B. Wang, M. G. Helander, J. Qiu, D. P. Puzzo, M. T. Greiner, Z. W. Liu and Z. H. Lu, Appl. Phys. Lett. **98**, 073310 (2011).
[24] R. R. Chance, A. Prock, R. Silbey, Adv. Chem. Phys. **37**, 1 (1987).
[25] S.-Y. Kim and J.-J. Kim, Org. Electron. **11**, 1010, (2010).

초 록

차세대 디스플레이 재료로 각광받는 유기발광소자(OLED)는 내부 물질의 높은 굴절률로 인해 약 75%의 빛이 소자 밖으로 나오지 못하고 소멸된다. 내부에 갇힌 빛을 추출하는 방법 중 하나인 광결정을 투명 전극과 유리 기판 사이에 삽입하는 방식은, 광결정의 주기적 배열 때문에 특정 방향으로 빛이 추출되는 단점을 가지고 있다. 이를 개선하기 위해 광결정 대신 비주기적 나노구조를 삽입하였다. 또한 나노구조의 재료로 안정한 무기물인 스핀온 글라스를 나노 임프린트 리소그래피 공정으로 제작하였다. 균일한 패턴 제작을 위해 폴리다이메틸실록세인 몰드 위에 스핀 온 글라스를 먼저 올린 나노 트랜스퍼 리소그래피를 사용하였다. 폴리머-무기 하이브리드 필름을 스핀 코팅으로 입혀서 기판을 평탄화 하였다. 소자는 정면 방향에서 7%, 적분구 측정으로 19%의 효율 증가를 보였다. 파장 전반적인 광추출 효율을 보였고, 방위각에 따른 소자의 발광 패턴은 동일하였다.

주요어: 유기발광다이오드, 비주기적나노구조, 상온 나노 임프린트 리소그래피, 스핀온 글라스, 폴리머−무기 하이브리드 필름
학 번: 2011-22874